J Mater Sci (2011) 46:6111–6117
DOI 10.1007/s10853-011-5575-8

Microstructure evolution of gold thin films under spherical indentation for micro switch contact applications

Brice Arrazat · Vincent Mandrillon · Karim Inal · Maxime Vincent · Christophe Poulain

Received: 18 November 2010 / Accepted: 19 April 2011 / Published online: 19 May 2011

Abstract RF MEMS (Radio Frequency Micro Electro Mechanical System) switches are promising devices but their gold-on-gold contacts, assimilated for this study to a sphere/plane contact, represent a major reliability issue. A first step toward understanding failure mechanisms is to investigate the contact metal microstructure evolution under static and cyclic loading. After static and cyclic loading of sputtered gold thin films under spherical indentation, high-resolution Electron Back Scatter Diffraction (EBSD) is used to investigate the contact area. Grain rotation against {111} fiber texture of 1-μm-thick sputtered gold thin film is a signature of plastic deformation. Grain rotation is observed above 1.6 mN under static loading using a spherical diamond indenter with 50-μm tip radius. The heterogeneity in grain rotation observed corresponds to a greater plastic deformation in the middle of the indent than at the edge. A 30° grain rotation due to cyclic work hardening is observed for a half-million mechanical cycles under 300 μN load using a spherical gold tip (20 μm radius). The same test in hot switching mode induces a grain growth in the contact area. Therefore, thermal effects occurring during hot switching are underlined.

B. Arrazat (✉) · V. Mandrillon · K. Inal
Ecole Nationale Supérieure des Mines de Saint-Etienne, Armines, Centre Microélectronique de Provence—Georges Charpak, Gardanne, France
e-mail: arrazat@emse.fr

B. Arrazat · V. Mandrillon · M. Vincent · C. Poulain
CEA-Léti, Minatec, Grenoble, France

M. Vincent
Division of Innovation, Schneider Electric Industries, Grenoble, France

Introduction

To keep up with the wide spectrum of telecommunication standards and demands of communicating objects, transceiver systems will be dynamically reconfigurable. The most common possibility by far consists in a switching matrix to direct the signal through a dedicated block. For that possibility, the Micro Electro Mechanical Systems (MEMS) switch is an attractive alternative to traditional FET (Field Effect Transistor) or p-i-n diode switches in applications where microsecond-switching speed is sufficient. A MEMS switch is composed of a mobile part (bridge or beam) and a contact area of a few μm^2 (flat or spherical bump) separated by an air gap (Fig. 1). The mechanical movement obtained using electrostatic, magnetostatic, piezoelectric, or thermal actuation is necessary to close the switch. These components show much lower insertion loss and higher isolation than their competitors [1].

Recent works on contact switch reliability revealed two primary failure mechanisms during cycling, which are contact resistance increase and stiction [2, 3]. Those mechanical degradations of contact are linked to contact material properties. Practically, gold is selected as the contact material due to low resistivity and low sensitivity to oxidation. However, gold's relative low hardness and low softening temperature seem to be the origin of contact degradation [2, 3].

To solve this problem, several studies are dedicated to alternative contact materials [2–4]. Preference is given to gold alloyed with platinum-group metals. Significant results are obtained showing sevenfold lifetime increases [3]. But the same failure mechanisms occur, so the morphology integrity is investigated to understand which mechanisms are at the origin of contact degradation. Yan et al. [5] demonstrate that the degradation area increases along with the increase in current intensity (from 70 to

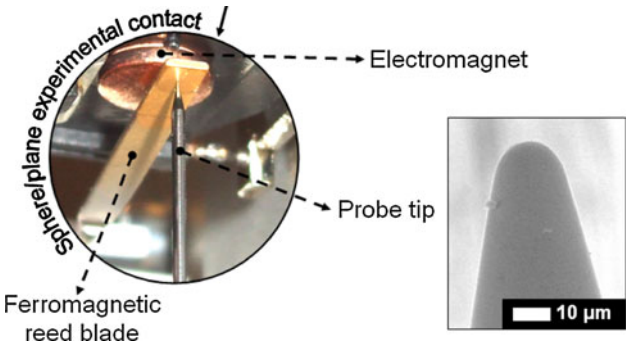

Fig. 1 Apparatus dedicated to cyclic loading test

350 mA). Also, the degradation area increases under mechanical cycling at a force of 200 µN as a function of the number of cycles, and is linked to an increase in contact resistance [6]. Gregori [7] investigates the deformation in the contact area and shows that partial flattening of asperities and pile-up formation occurs with actuation. Curvature radius of asperities and mechanical properties (elasticity and hardness) of material are major parameters of adhesion force [8], and the evolution of adhesion force could explain stiction mode of failure.

In this study, after static and cyclic loading of sputtered gold thin films under spherical indentation, high-resolution Electron Back Scatter Diffraction (EBSD) is used to investigate microstructural changes in the contact area. Complementary Atomic Force Microscopy (AFM) topography characterization (pile-up, indent diameter, asperity curvature radius) of the contact area is performed. Localized nanoindentation measurement of hardness evolution linked to observed structural changes is also performed.

Sample description

The sample consists of the following sputtered thin film stack deposited on a silicon substrate: 1 µm of gold/50 nm tungsten nitride diffusion barrier/20 nm tungsten adhesion layer. The rms roughness of the investigated gold surface is 5 nm. The average peak-to-valley is 35 nm. The average curvature radius of asperities on gold thin film is 240 nm.

Recent studies [9] have demonstrated the maturity of EBSD in field emission scanning electron microscope (FEGSEM). High spatial resolution as small as 10 nm is reached. Penetration depth into gold thin films is around 10 nm. Crystallographic texture and grain boundary rotation of surface are determined and quantified. A strong {111} fiber texture normal to the gold surface is exhibited with an average 90-nm grain size.

A Nanoindenter XP from MTS instruments was used to determine mechanical properties of the gold thin film using the dynamic contact module (DCM) option and a Berkovich indenter tip. The continuous stiffness measurement (CSM) technique allows the measurement of dynamic stiffness continuously throughout the loading segment by superimposing a small dynamic oscillating displacement to the quasi-static force by means of a frequency-specific amplifier. The oscillation displacement was 1 nm, the frequency was 50 Hz and the strain rate was constant (0.05 s^{-1}). The area function of the Berkovich tip was obtained by the indentations on fused silica in the range of 10–300 nm indentation depth, i.e., displacement as suggested by [10].

Mechanical solicitations

In this study, ten static loads ranging from 50 µN up to 130 mN are applied on the gold thin film at different locations, using the nanoindenter with a spherical diamond tip of 50 µm radius in order to be representative of micro-switch contact pressure (Table 3). These experiments proceed as follow: after surface contact, the load increases with a constant strain rate (0.05 s^{-1}). The targeted load is applied during 1 s, then unload occurs at the same strain rate.

To perform mechanical cycling in the same pressure range, an apparatus developed by Vincent [11] is used for endurance testing in both hot and cold switching mode under constant voltage. In cold switching mode, the voltage between the probe and the gold film is only applied when the switch is closed, while the voltage is always applied in hot switching mode, leading to closure, and opening electrical effects. This apparatus is constituted by a commercial ferromagnetic reed blade (flexible beam) where the sample is glued and put into contact with a 20-µm curvature radius gold probe using a piezoelectric actuator that has a displacement resolution of 10 nm, as shown in Fig. 1. The applied load is measured using a strain gage force sensor with 20 µN resolution. After first contact and load adjustment, an electromagnet located above the ferromagnetic beam is used for cyclic contact opening/closing actuation under sinusoidal excitation. Load, switching frequency, voltage, and current compliance are, respectively, fixed to 300 µN, 10 Hz, 5 V, and 1 mA (Table 2).

In order to have a comparison criterion between the mechanical solicitations under static loading, cyclic loading and a real micro-switch, the equivalent average contact pressure (P_{eq}) corresponding to the applied load F is introduced and calculated from Hertz equation for a sphere/plane elastic contact (Eq. 1).

$$P_{eq} = \frac{1}{\pi}\left(\frac{4E_{eq}}{3R}\right)^{2/3} F^{1/3} \quad (1)$$

E_{eq} and R are, respectively, the effective elastic modulus and curvature radius of the indenter tip. The former is related to material properties by the following relationship:

$$\frac{1}{E_{\text{eq}}} = \frac{1-\upsilon_i^2}{E_i} + \frac{1-\upsilon_f^2}{E_f} \quad (2)$$

E and υ are Young's modulus and Poisson's ratio, subscripts f and i corresponding, respectively, to the film and to the indenter tip. Young's modulus and Poisson's ratio value for the gold thin film are $E_f = 80$ GPa (experimental) and $v_f = 0.44$. Table 1 shows the calculated effective elastic modulus for the different spherical indenter types.

In the following part of the article, the hertzian equivalent average contact pressure is always used. Load applied in a micro switch is about 10 μN. Therefore, for a contact bump curvature radius of 10 μm, the MEMS switch pressure is around 240 MPa. Endurance cycling experiments are carried out at 470 MPa (Table 2). On different test areas, 26 thousand cycles are performed in hot switching mode and a half-million cycles are performed in cold switching mode (Table 2).

Static loads applied by spherical indentation are summarized in Table 3. The range of MEMS switch pressure is investigated at low loads. At high loads, pressures above 1 GPa allow a high degradation analysis, but obviously do not correspond to the real applied pressure because of contact plastic deformation and substrate effect.

Static loading analysis

The geometry of the residual indent mark that is created under static loading by the spherical indenter tip (Table 3) at the contact location is determined by AFM measurement. The diameter and depth of spherical indent and pile-up height are defined in Fig. 2. The indent depth (h) is defined as the difference between reference plane and bottom of indent. The pile-up height (s) is defined as the difference between top of pile-up and reference plane. A gaussian filter is used to remove the short wavelength components as shown in Fig. 2. The diameter of the residual imprint obtained during indentation increases with applied pressure (Fig. 3). It is observed that this increase in diameter follows the classic plastic model [12], where the hardness equals the ratio between the load and the projected contact area, such that the hardness equals 0.92 GPa to be compared with hardness measured by standard nanoindentation using a berkovitch tip (cf §2). In Fig. 3, the experimental data are represented by points and the plastic model, by a red line.

Experimentally, indent marks created under pressures lower than 400 MPa (or 335 μN) are difficult to quantify by AFM measurement. Only some asperities are partially hammered. The limit of detection corresponds to Tabor condition, where plastic deformation starts over the third part of hardness. Around 500 MPa (or 650 μN), the roughness in the center of indent is around 4 nm and close to the gold thin film value of 5 nm (Fig. 4). When the pressure increases above 500 MPa (or 650 μN), the roughness decreases drastically to less than 2 nm due to plastic deformation. Before solicitation, the average curvature radius of asperities on gold thin film is around 240 nm. Above 500 MPa (or 650 μN) of applied pressure, the average curvature radius of the asperities in the middle of the indent is 850 nm, showing huge plastic deformation of asperity summits added to global plastic deformation. The same evolution of the roughness and of the curvature radius of asperity after twelve million cycles under 180 μN in [7] is found, corresponding to an increasing propensity for permanent adhesion.

The pile-up formation is observed above 650 μN, corresponding to 500 MPa (Fig. 5). The ratio (s/h) of pile-up height on indent depth increases from 0 to 0.5 with pressure applied. This is due to the transition from purely elastic deformation at low pressure to plastically dominated behavior at high pressure [13]. The pile-up is a signature of thin-film global plastic deformation.

The previous indents, already analyzed by AFM, are investigated by EBSD characterization as shown Fig. 6. Comparison of both images demonstrates the one-to-one equivalency between topographic asperities with the grain shapes observed by EBSD. As previously shown, gold thin

Table 1 Young's modulus, Poisson's ratio, and radii of different indenter types and their effective elastic modulus

	E_i (GPa)	v_i	R (μm)	E_{eq} (GPa)
Gold-on-gold micro-switch	80	0.44	~10	49.6
Spherical indenter (static)	1140	0.07	50	91.3
Spherical gold probe (cyclic)	80	0.44	20	49.6

Table 2 Cyclic loading, calculated pressure, and number of cycles of tests performed

Cycling conditions	Hot switching (5 V, 1 mA, 10 Hz)	Cold switching (5 V, 1 mA, 10 Hz)
Cyclic loading (mN)	0.3	0.3
Pressure (MPa)	470	470
Number of cycles	26,000	500,000

Table 3 Static loads and calculated pressures applied by spherical diamond indentation (radius 50 μm)

Static loading (mN)	0.05	0.22	0.55	1	1.6	7	18	37	73	130
Pressure (MPa)	210	350	470	580	670	1100	1500	1920	2410	2920

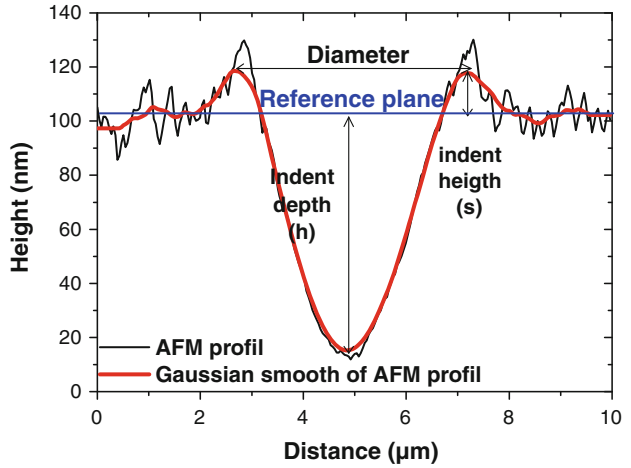

Fig. 2 Typical AFM profile of one of the indent imprint created during indentation

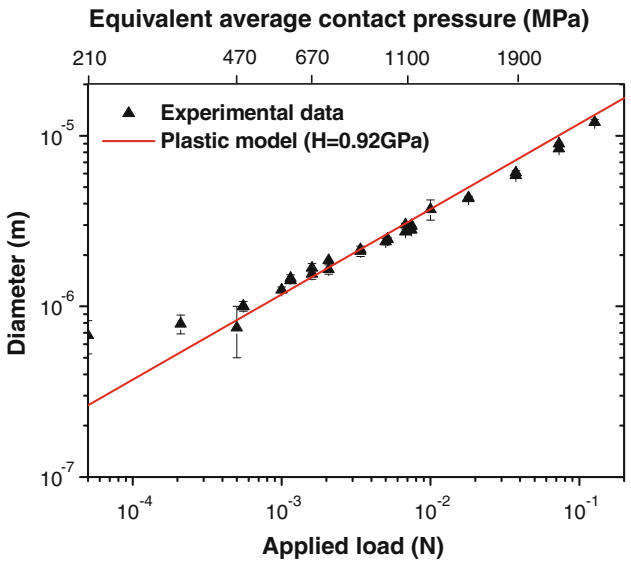

Fig. 3 Diameter (m) versus equivalent pressure (Pa) and applied load (N) of spherical indentation (50 µm tip radius) in gold thin film

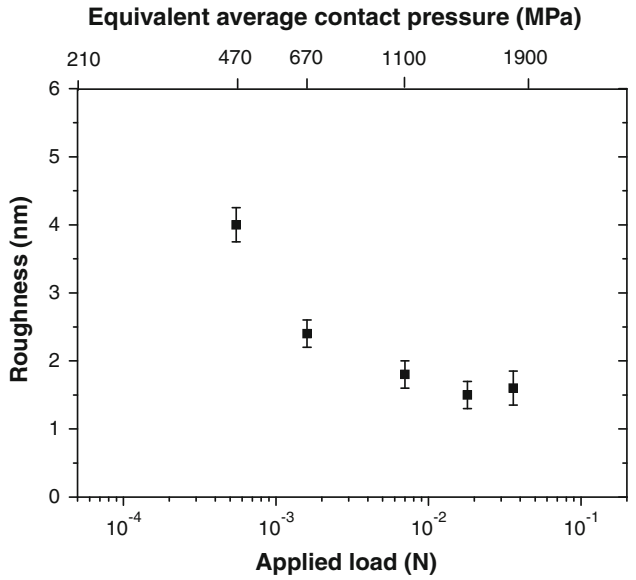

Fig. 4 Root mean square roughness (nm) in the middle of the indent mark versus applied pressure (Pa) and load (N) after static loading spherical indentation

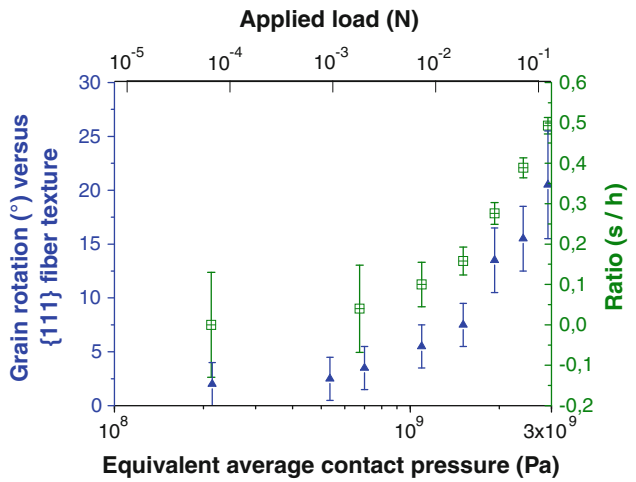

Fig. 5 Ratio s/h between height of pile-up and indent depth, and grain rotation relative to {111} fiber texture as a function of equivalent average contact pressure (Pa) and applied load (N) of spherical indentation (50 µm radius) in the gold thin film

film has a strong {111} fiber texture. The grain circled in Fig. 6 at the middle of the indent mark obtained under a 1.6 mN static load suffers 10° of rotation in comparison to the {111} initial fiber texture. Only grains in the middle of indent present a rotation. Observed deformation is therefore heterogeneous. To determine average grain rotation as a function of average pressure, a 1×1 µm^2 area is analyzed for each indent. No grain size modification is observed on any indent. Rotation angle of grains increases with pressure above 500 MPa (Fig. 5). This rotation reaches 21° under an equivalent pressure of 3 GPa (or 130 mN). Both the ratio (s/h) between pile-up height and indent depth and the grain rotation follow the same evolution with applied pressure, and are representative of the level of plastic deformation (Fig. 5). These rotations induce the {111} fiber texture degradation. The central spot and external fringe on the {111} pole figure are larger. In extreme cases, the central spot transforms into a circle. This type of crystallographic texture deformation is also observed on polycrystals under uniaxial compression [14]. This grain reorientation can be predicted by a Taylor-type model of crystalline plasticity [14].

This demonstrates that EBSD analysis provides precious information on plastic deformation level. Therefore, this

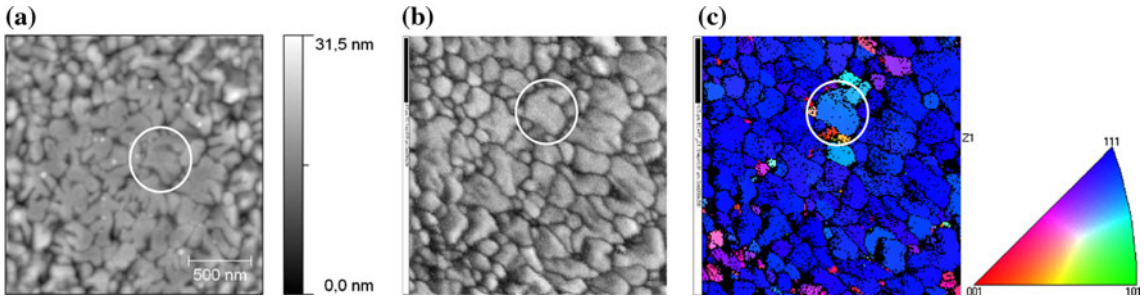

Fig. 6 2 × 2 μm^2 AFM flattened top view (**a**), EBSD band contrast map (**b**), and crystallographic orientations (**c**) of indent mark at 1.6 mN static load. EBSD maps have a size of 2 × 2 μm^2 with a step of 10 nm (around 75% of points are indexed). *Circled grain* shows a 10° rotation due to contact

characterization technique will be applied on cyclic loading contact areas with interest.

Cyclic loading mode analysis

A half-million cold switching cycles are performed as detailed in Table 2. The setup of this experiment needs a first contact approach with the piezoelectric actuator. This first contact force is around 1 mN and induces a grain rotation of 10° (Fig. 7c). After the approach, mechanical cycling under a 300 μN (or 470 MPa) load is performed by the sinusoidal signal sent to the electromagnet. A grain rotation of 30° is observed after a half million cycles. This is due to cumulative plastic deformation. The grain rotation obtained is higher than under 3 GPa (or 130 mN) static loading equivalent contact pressure. The {111} pole figure obtained has a strong crystallographic texture and is slightly different from static loads. First, contact approach induces a shift of the {111} texture fiber. Then, mechanical cycling induces a larger central spot and external fringe on the {111} pole figure.

The same test is performed in hot switching mode. Grain boundary rotation obtained for 26,000 hot switching cycles is around 25°, i.e., of the same order as after a half-million-cycle cold switching experiment. Moreover, the resulting crystallographic texture of the contact area is extremely different from previous tests. A strong degradation of the {111} fiber texture is observed but no particular orientation is predominant (Fig. 7d). The grain size has increased in contact area, as shown in Fig. 8. The average grain size is around 250 nm, whereas initial average grain size of gold thin film is around 90 nm. Thermal energy produced during by hot switching (arcing or melting) induces an abnormal recrystallization. The grain size increase and the resulting crystallographic texture differ from previous solicitations

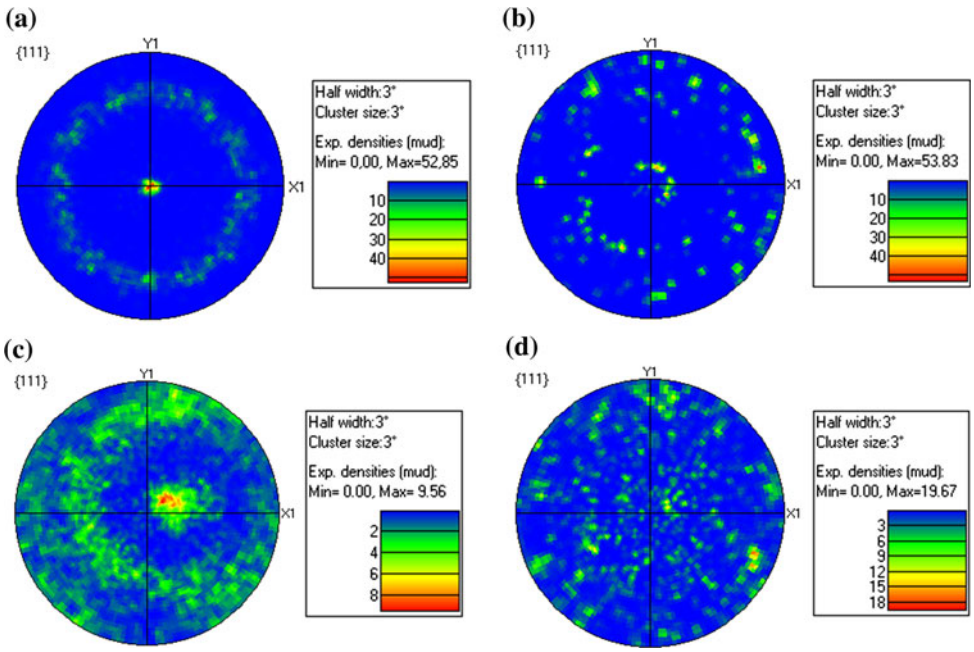

Fig. 7 {111} pole figure of initial gold thin film (**a**), after a 73 mN static loading (**b**), after half-million cold switching cycles under 300 μN (**c**), and after 26 thousand hot switching cycles under 300 μN (**d**)

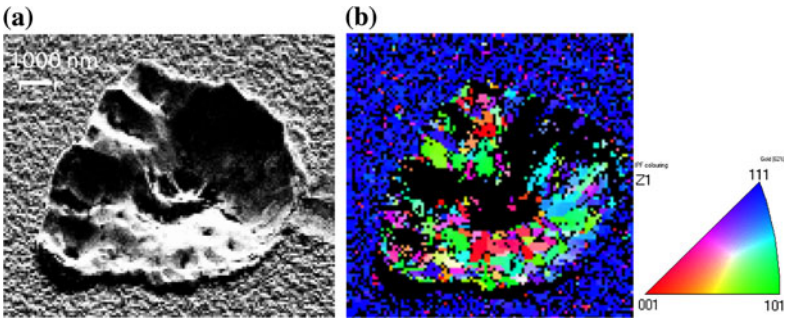

Fig. 8 Scanning electron microscopy image (**a**) and EBSD map (**b**) of 26 thousand hot switching cycles contact area under 300 μN load. EBSD map have a size of 20×20 μm^2 with a step of 100 nm (52% of points are indexed)

and is the expression of a different mechanism of degradation.

A single nano-indentation in the cold and hot switching degradation area is performed to investigate the hardness (Fig. 9). These measurements are compared to the average of 64 indentations conducted on gold thin film and presented in Fig. 9. At a depth of 150 nm, the hardness of the gold thin film is 1.6 GPa. On an area subjected to a half-million quasi cold switching cycles at 150 nm of depth, the measured hardness increases by 12% compared to the initial gold thin film. No grain size modification was observed on an area subjected to a half-million quasi cold switching cycles. This increased hardness could be due to surface strain hardening. On an area subjected to 26,000 hot switching cycle at a depth of 150 nm, the measured hardness decreases by 22% compared to the initial gold thin film. This decrease in hardness could correspond to the Hall–Petch effect described by the following relation:

$$H = H_0 + K_H d^{-1/2} \quad (3)$$

where H_0 and K_H are experimental constants and d is the average grain size (Eq. 3). More experiments in hot switching mode should be addressed to use this relation. A

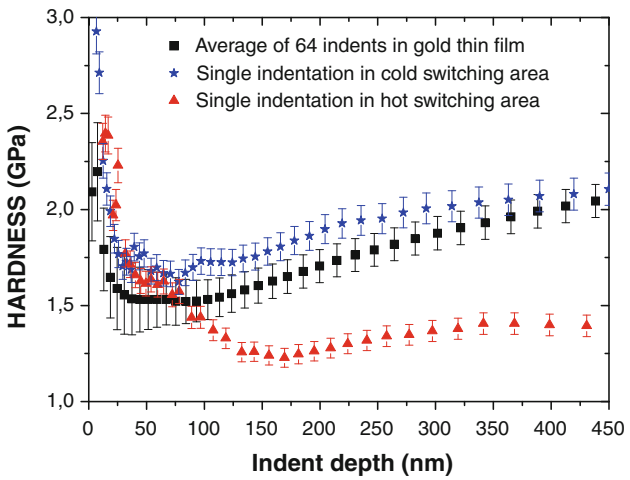

Fig. 9 Gold thin film hardness measurement as a function of depth before and after contact loading

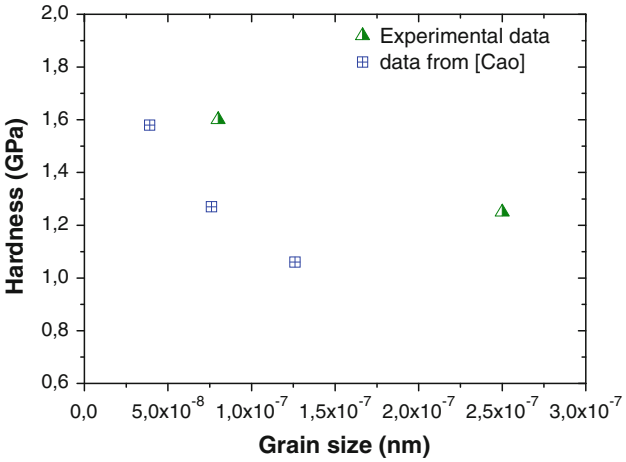

Fig. 10 Measured hardness versus grain size

comparison with the results obtained in Cao study [15] concerning the decrease of gold hardness with grain size is presented in Fig. 10.

Conclusions

This study demonstrates the interest of EBSD analysis for micro-switch reliability study. The authors have highlighted the following points:

- The {111} pole figure evolution shows grain rotation due to plastic deformation, with good correlation with pile-up intensity.
- The {111} pole figure gives information about the type of solicitation: compression.
- The grain size determined by EBSD leads to the confirmation that thermal events occurring during hot switching are strong enough to concern the grain volume and to induce grain growth.
- The hardness measurements are coherent with the microstructural evolution observed by EBSD.

Other points should be addressed to improve EBSD analysis and will be implemented in further studies. A

crystallographic plastic model can be used to predict microstructural evolution. The same type of analysis will be performed on the contact area of a real micro switch, and then EBSD analysis should be performed on the contact area cross-section.

References

1. Rebeiz GM, Muldavin JB (2001) IEEE Microwave Mag 2(4):59
2. Coutu RA, Kladitis PE, Starman LA, Reid JR (2004) Sensors Actuators A 115(2–3):252
3. Coutu RA, Reid JR, Cortez R, Strawser RE, Kladitis PE (2006) IEEE Trans Compon Packag Technol 29(2):341
4. Chen L, Lee H, Guo ZJ, McGruer NE, Gilbert KW, Mall S, Leedy KD, Adams GG (2007) J Appl Phys 102(7):074910
5. Yan X, McGruer NE, Adams GG, Majumder S (2003) In: 12th International conference on transducers, solid-state sensors, actuators and microsystems, Boston
6. Chen L, Guo ZJ, Du Y, McGruer NE, Adams GG (2006) IEEE Microwave Mag
7. Gregori G, Clarke DR (2006) J Appl Phys 100(9):094904
8. Duvivier PY, Mandrillon V, Inal K, Dieppedale C, Deldon-Martoscia S, Polizzi J (2010) In: 2010 Proceedings of the 56th IEEE Holm conference on electrical contacts, Minneapolis
9. Humphreys FJ (2001) J Mater Sci 36(16):3833. doi:10.1023/A:1017973432592
10. Pharr GM, Strader JH, Oliver WC (2009) J Mater Res 24(3):653
11. Vincent M, Chiesi L, Rousset P, Lapiere C, Poulain C, Carbone L, Houze F, Delamare J (2009) In: 2009 Proceedings of the 55th IEEE Holm Conference on electrical contacts, Vancouver
12. Fischer-Cripps AC (2004) In: Nanoindentation, Springer-verlag, New York
13. Pharr GM, Taljat B (2004) Int J Solids Struct 41:3891
14. Kalidindi SR, Bronkhorst CA, Anand L (1992) Phil Trans R Soc Lond 341:443
15. Cao Y, Allameh S, Nankivil D, Sethiaraj S, Otiti T, Soboyejo W (2006) Mater Sci Eng A 427(1–2):232